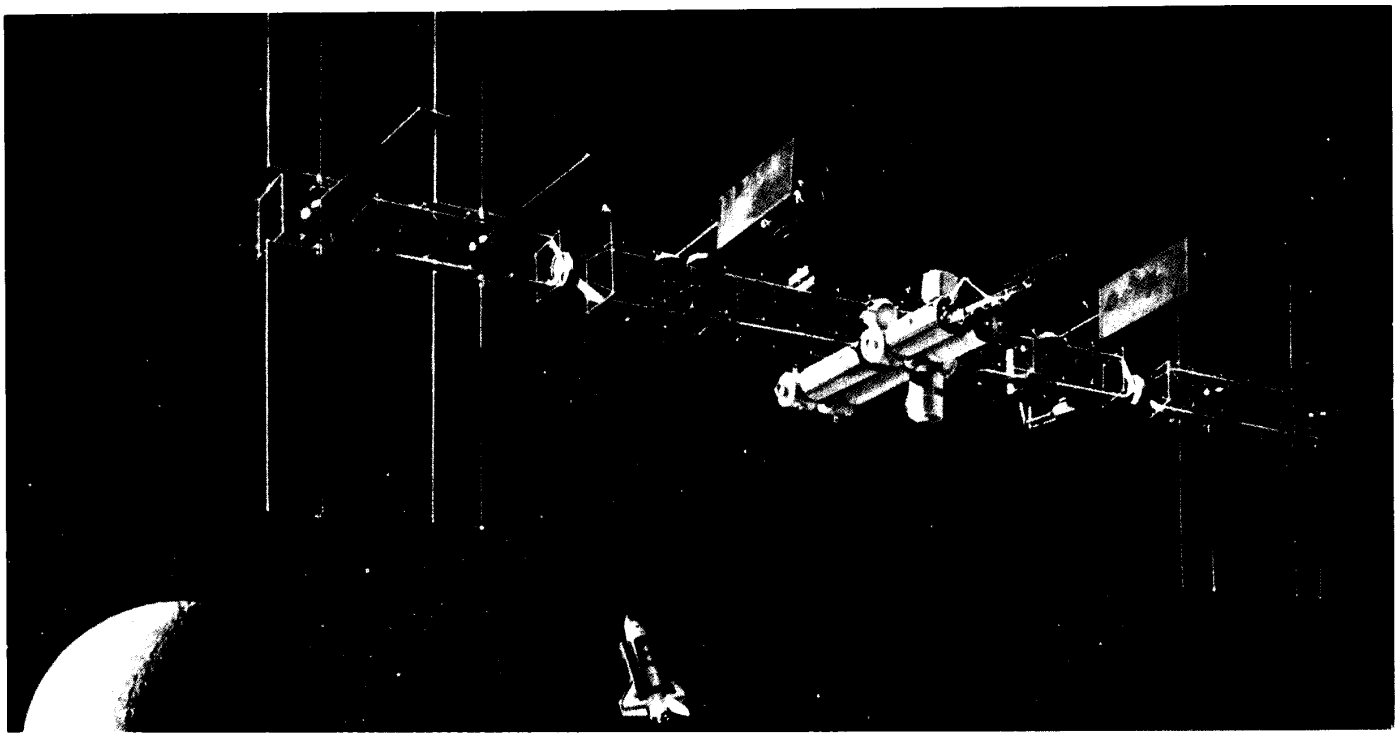

NASA

Robust Controllers for Space Station Momentum Management

Michael R. Elgersma, Gunter Stein, Michael R. Jackson, and John Yeichner

This paper describes the design of controllers for space station attitude control and momentum management. The controllers stabilize the unstable gravity gradient torques, keep attitudes and momentums due to aero disturbance torques small, and are robust to uncertainties in the moments of inertia of the space station. Structured singular values of the closed loop system are computed to verify the robustness of the controllers.

Space Station Freedom

Space Station Freedom is a large manned orbiting platform, scheduled for operation in the mid 1990s. The station will operate in a nominal earth pointing orientation, gravity gradient unstable, and at altitudes where significant aerodynamic disturbances cause large momentum buildup in its control moment gyros. This momentum will be maintained within tolerable levels by balancing aero torques with gravity gradient torques. This gives rise to some fundamental control performance tradeoffs between stabilization, attitude regulation, and momentum magnitudes. This article explores these tradeoffs using H-infinity optimization. It also describes simplified controllers which achieve near-optimal performance with good robustness properties and with significantly reduced complexity. Reference [1] addresses some of the nonlinear issues associated with the control of the space station.

Presented at 1991 IEEE Conference on Decision and Control, Brighton, England, December 11-13, 1991. *Michael R. Elgersma, Gunter Stein, and Michael R. Jackson are with Honeywell SRC, MS MN65-2500, 3660 Technology Drive, Minneapolis, MN 55418. Gunter Stein is also an Adjunct Professor at the Massachusetts Institute of Technology. John Yeichner is with Honeywell SASSO, MS FL51-351-4A, Clearwater, FL 34624-7290.* *This work was supported by the McDonnell Douglas Corporation under a Space Station contract to Honeywell Inc.*

Background

Nominal Orientations

As the space station orbits the earth, the attitude controller attempts to keep it aligned with the rotating local vertical local horizontal (LVLH) reference frame. The LVLH reference frame is centered at the c.g. of the space station, the x axis points along the flight path, the y axis is aligned with the normal to the orbit plane, and the z axis is pointed towards the center of the earth (see Fig. 1).

The LVLH orientation of space station facilitates the operation of antennas, star sensors, and other fixed experimental packages. However, the solar panels must be kept pointed towards the sun for maximal

 0272-1708/92/$03.00©1992IEEE

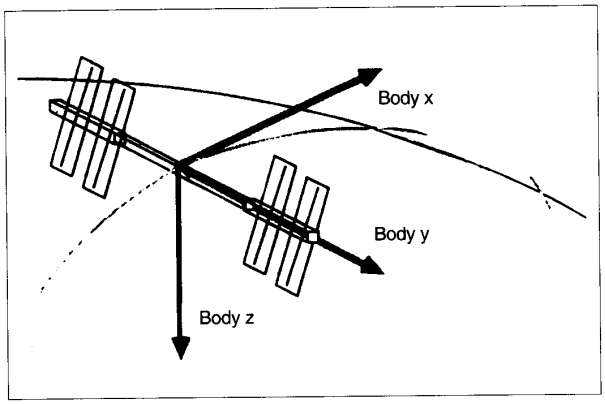

Fig. 1. Space station in local vertical local horizontal frame.

efficiency, so they are mounted on rotating joints to keep their attitude inertially fixed.

Dynamics

The space station rigid body attitude dynamics and kinematics are given by the following vector equations where the parameters and variables are: J (Body moment-of-inertia matrix), $E = [\underline{e}_x\, \underline{e}_y\, \underline{e}_z]$ (Rotation matrix from LVLH to body), $\underline{\omega}$ (Body angular rate w.r.t. inertial), $\underline{\omega}_0$ (LVLH angular rate w.r.t. inertial), $\omega_0 = ||\underline{\omega}_0||$ (Orbital rate, approx 0.0011 rad/s), and $\underline{T}_c$ $\underline{T}_d$ (Control and disturbance torques):

$$\begin{aligned} J\dot{\underline{\omega}} + \underline{\omega} \times J\,\underline{\omega} &= 3\omega_0 2\underline{e}_z \times J\underline{e}_z + \underline{T}_c + \underline{T}_d \\ \dot{\underline{e}}_i + (\underline{\omega} - \underline{\omega}_0) \times \underline{e}_i &= 0 \qquad i = x,\ y,\ z \end{aligned} \tag{1}$$

The term in (1) with coefficient 3 is the first order term in the gravity gradient torque. It is due to the fact that the gravitational pull of the earth is stronger on parts of the station that are closer to the earth. This torque is destabilizing when the long boom of the station is normal to the orbit plane: if one end tips down towards the earth, the gravity gradient torque will pull it down further. Note that rotation of the station about the LVLH z axis does not alter the distance of any part from the earth, so there is no gravity gradient torque about the z axis.

Disturbances

The large cross sectional area of the solar panels causes large drag forces on the station. Roughly speaking, atmospheric particles experience inelastic collisions with the panels, transferring all of their momentum to the station. The resulting aero force direction is in the opposite direction of the velocity vector.

The aero force $\underline{F}_{\text{aero}}$ is shown where the parameters and variables are: ρ (Atmospheric density), $\underline{S}$ (Panel area times unit normal vector), $\underline{V}$ (Space station velocity):

$$\underline{F}_{\text{aero}} = -\rho|\underline{S}^T\underline{V}|\underline{V} \tag{2}$$

The aero torque $\underline{T}_{\text{aero}}$ is equal to the cross product of the aero force $\underline{F}_{\text{aero}}$ with the distance vector $\underline{r}_{\text{cg-cp}}$ from the center of gravity to the center of pressure on the station:

$$\underline{T}_{\text{aero}} = \underline{r}_{\text{cg-cp}} \times \underline{F}_{\text{aero}} \tag{3}$$

The magnitude of the aero force is proportional to the component of the solar panel surface normal in the direction of the velocity vector. Since the panels are inertially fixed, while the velocity is fixed in the rotating LVLH frame, the magnitude of the aero force has a sinusoidal time variation. During each half orbit cycle an opposite face of the solar panel is struck by the atmosphere, so the sinusoidal time variation is actually rectified (therefore the absolute value in (2)). The dominant terms in the Fourier series of this rectified sine wave are the DC and twice orbit rate terms. The atmospheric density also varies during each orbit since the heat from the sun expands the earth's atmosphere, bringing more of it up to the altitude of the space station (this expansion of the atmosphere is called the diurnal bulge). The dominant terms in the Fourier series of the density are the DC and orbital rate terms. The aero torque $\underline{T}_{\text{aero}}$ can then be represented as a periodic external disturbance with dominant terms at DC, orbit rate and twice orbit rate.

The net result is large disturbance torques at DC (4 ft-lbs), at orbit rate (1 ft-lb at 0.001 rad/s), and at higher orbit rate harmonics.

Control Torques

Control torques for the attitude control system come from reaction control system (RCS) thrusters, and from control moment gyros (CMG). A CMG is a large spinning flywheel whose momentum $\underline{H}$ has constant magnitude. The direction of the momentum vector can be turned by applying a torque $\underline{T}_{\text{CMG}}$, to the CMG. The reaction torque $\underline{T}_c$ on the space station has opposite sign:

$$\begin{aligned} \dot{\underline{H}} + \underline{\omega} \times \underline{H} &= \underline{T}_{\text{CMG}} \\ T_c &= -\underline{T}_{\text{CMG}} \end{aligned} \tag{4}$$

Because this mechanism of torque generation expends no fuel, the CMGs provide the baseline actuation mode for long-term station operations. In other words, the control moment gyros move back and forth to maintain the orientation of the space station.

CMG Control Requirements

The control laws which command CMG torques are called the attitude and momentum management system. This system is required to stabilize the station against unstable gravity gradient torques, to maintain attitude errors and CMG momentum accumulation within acceptable bounds, and to reject strong periodic disturbances caused by the rotation of the solar panels and by variation in atmospheric density associated with the diurnal bulge.

The system must also be robust with respect to uncertainties in the station's moments of inertia and its flexible dynamics. The primary moment of inertia variations come from changes during the buildup sequence, from movable payloads, and uncertainties in the moments of inertia of the station itself. These combined effects can be quite large. Flexible dynamics on the other hand, do not pose significant robustness problems. The lowest flex modes of the station are approximately 0.6 rad/s, which is approximately 60 times greater than the needed control bandwidth (~10 times orbit rate) and leaves ample room for gain stabilization Plots of flex dynamics can be seen in [2].

Linearized Equations of Motion

Linearized equations of motion are derived in [3]. The angles and rates $\underline{\theta}$, $\dot{\underline{\theta}}$ are between the LVLH reference frame and a body reference frame nominally aligned with LVLH. In this new set of axes, $\underline{\theta} = \underline{0}$ at

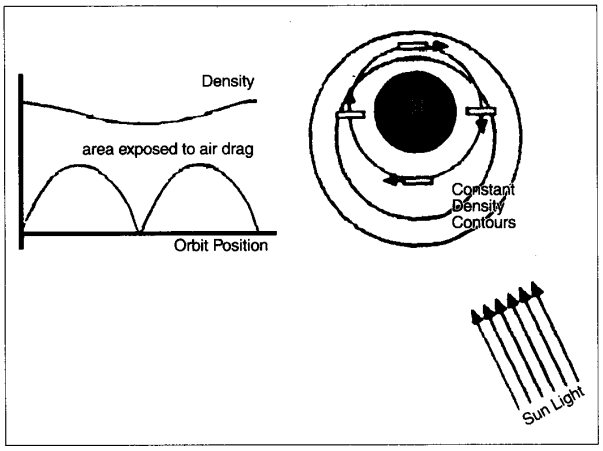

Fig. 2. Graphical illustration of aerodynamic disturbances.

equilibrium, J is not diagonal, and the linearized attitude equations are given by the following where J is the 3×3 matrix representing the inertia of the space station in the body reference frame, $\ddot{\underline{\theta}}$ is the 3×1 vector representing angular acceleration, ω_0 is the nominal rotation rate, $\underline{T}$ is the 3×1 vector representing torque applied by the outside forces and the internal control, $L(J)$ is a 3×6 matrix whose left 3×3 submatrix multiplies $\omega_0 \dot{\underline{\theta}}$ under to give coriollis torques (due to the orbit of the space station around the earth), and the right 3×3 submatrix of $L(J)$ multiplies $\omega_0 2\ \underline{\theta}$ under to give gravity gradient and centrifugal torques:

$$J\ddot{\underline{\theta}} = L(J)\begin{bmatrix}\omega_0\dot{\underline{\theta}} \\ \omega_0^2\underline{\theta}\end{bmatrix} - \underline{T} \tag{5}$$

The diagonal elements of the J matrix are labeled J_{xx}, J_{yy}, and J_{zz}. Because of large numerical ranges in this model, it is often convenient to normalize time by ω_0 and inertia by J_{zz}. In this new set of units, $\omega_0 = 1$, $J_{xx} \approx 0.95$, $J_{yy} \approx 0.14$, and $J_{zz} = 1$.

Control System Designs

This section describes two control system design approaches which are being used to synthesize control laws for the competing requirements outlined above. The first approach is based on the formal H-infinity optimization theory developed over the last several years. Details of the H-infinity derivations can be found in in [4]. This approach was used to explore fundamental tradeoffs between the various control objectives and to rapidly produce controllers for high level station configuration tradeoffs and operation procedures. The second approach is more classical in nature, consisting of separate inner-loop attitude control and outer-loop momentum management designs. This approach produces simpler controllers, easier to schedule with mass property variation, yet possessing performance very close to the formal optimal designs, with good robustness properties.

H-Infinity Designs

The overall design tradeoff between stabilization, attitude regulation, and momentum management is illustrated in Fig. 3. We have three attitude errors $\underline{\theta} = (\phi, \theta, \Psi)$ in roll, pitch and yaw, three momentum components $\underline{H}$ accumulated in the CMGs, and three control torque components $\underline{T_c}$ produced by the CMGs. The objective is to design control compensators $K(s)$, which keep these variables reasonably small in the face of specified disturbance torques $\underline{T_d}$. Expressed in recently popularized jargon, we want the map:

$$W_d^{-1}\ T_d \rightarrow (W_a\underline{\theta},\ W_h\underline{H},\ W_cT_c)$$

to be small, and we choose its H-infinity norm to be the criterion of smallness. As usual, the weighting functions, (W_a, W_h, W_c, W_d), can be freely adjusted and serve to explore the tradeoffs between the various signals in the design problem.

Fig. 4 illustrates a typical design trial using the H-infinity formalism. The figure shows singular value plots of closed loop frequency response matrices from $\underline{T_d}$ to $\underline{H}$ and $\underline{T_d}$ to $\underline{\theta}$, for a case with uniform (constant) weights selected to place heavy emphasis on momentum, less emphasis on attitude errors, and limiting bandwidth to approximately $10 \times$ orbit rate. (In normalized units, the weights are $W_a = 1$, $W_h = 1$, $W_c = 0.3$, $W_d = 1$.) The results show that a minimum momentum storage capacity of approximately 2500 ft-lb-s/ft-lb is needed to deal with broad-band disturbances, and that the associated attitude errors are as large as 0.05 rad/ft-lb (3°/ft-lb).

The momentum requirements from this example can be viewed as one of the costs of operating the station in unstable gravity gradient orientations. Stable orientations make the corresponding momentum plot vanishingly small. It also turns out that the attitude error level from

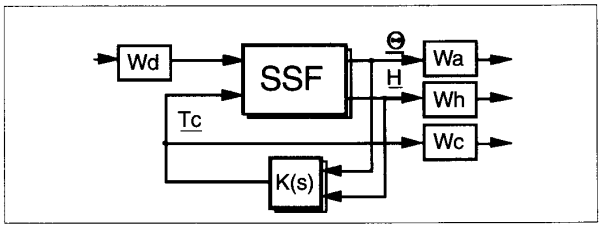

Fig. 3. Overall design tradeoffs.

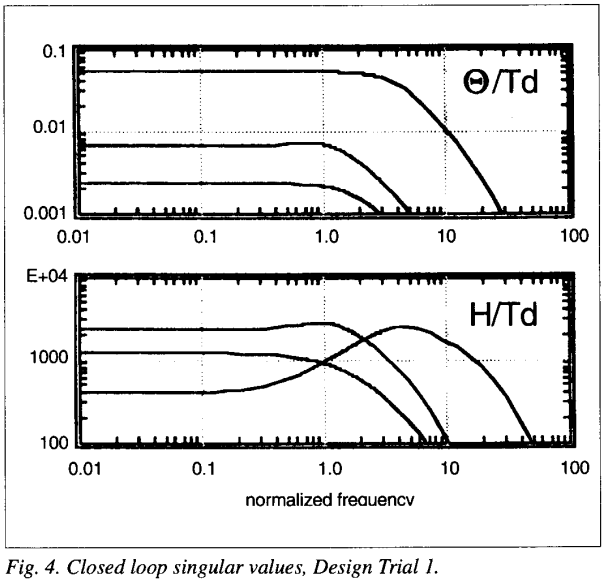

Fig. 4. Closed loop singular values, Design Trial 1.

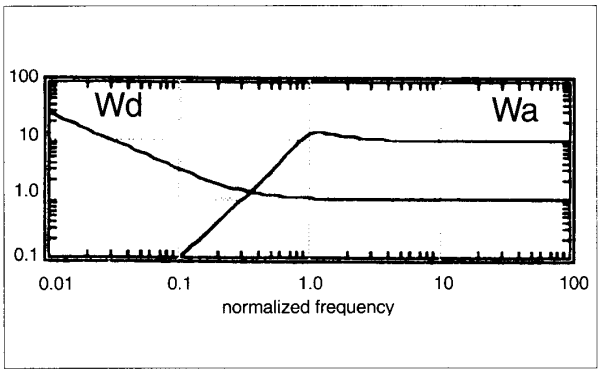

Fig. 5. Weights for Design Trial 2.

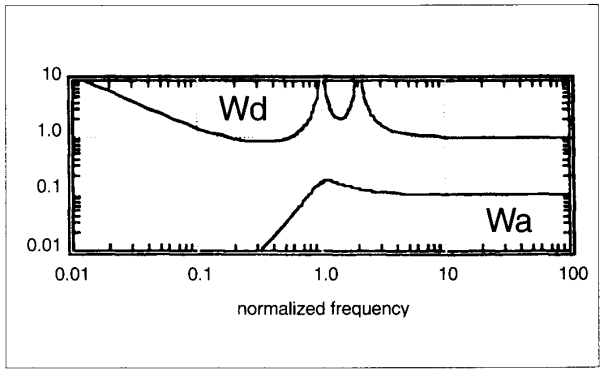

Fig. 7. Weights for Trial 3.

the example cannot be reduced (uniformly across frequency) even with much more emphasis placed on attitude and much less on momentum. This happens because the station's fixed gravity gradient coefficients require the same average offset angles to balance DC disturbance torques, regardless of $K(s)$. As seen in Fig. 4, one attitude direction is particularly bad in this regard, requiring ten times larger offsets than the other two. This bad direction corresponds to the pitch axis, for which the station's gravity gradients are very weak. Indeed in some early stages of the station's build sequence, the pitch axis terms are so weak that an alternate control strategy, so-called yaw bias control, must be used to control pitch during those stages. The yaw-bias control strategy is described in [5].

A second design trial more closely resembling the final control configuration is shown in Fig. 6. In this trial, the strong DC components of aerodynamic disturbances are explicitly modeled in the weight W_d, and the above mentioned attitude limitations are acknowledged by rolling off W_a at low frequencies. Frequency response magnitudes of these modified weights are shown in Fig. 5. The remaining weights again have constant values: $W_b = 1$, $W_c = 3.0$.

Fig. 6 shows that the controlled system's momentum responses can be entirely suppressed at DC where disturbances are concentrated, and that attitude errors can be made quite small at orbit rate and above. However, this is only accomplished at the expense of much larger momentum responses elsewhere in the frequency range. Note that 5000 ft-lb-sec/ft-lb capacity is needed at sub-orbital rates. This can again be viewed as a cost of operating in unstable gravity gradient orientations.

As a consequence of the large suborbital momentum peaks in Fig. 6, the station will exhibit large momentum transients, lasting several orbits, whenever the system is initialized and/or whenever discrete disturbance changes occur. In final steady state, of course, the momentum responses will be small. Because the station is expected to operate in steady state for the majority of its mission life, occasional large momentum transients are considered acceptable and will be managed with RCS assist whenever they threaten to exceed the storage capacity of the CMGs.

Still another H-infinity design trial is shown in Fig. 8. In addition to the DC disturbance model from above, this trial includes models for strong disturbance components at orbital rate and its first harmonic. The new weight W_d is shown in Fig. 7. For the remaining weights, W_a was scaled from Trial 2 by 1/100 to emphasize momentum, and W_h and W_c were left unchanged.

Design Trial 3 confirms that the controlled system's momentum responses can be suppressed not only at DC but at any frequency distinct from the undamped libration frequencies (see [5]). Of course, the

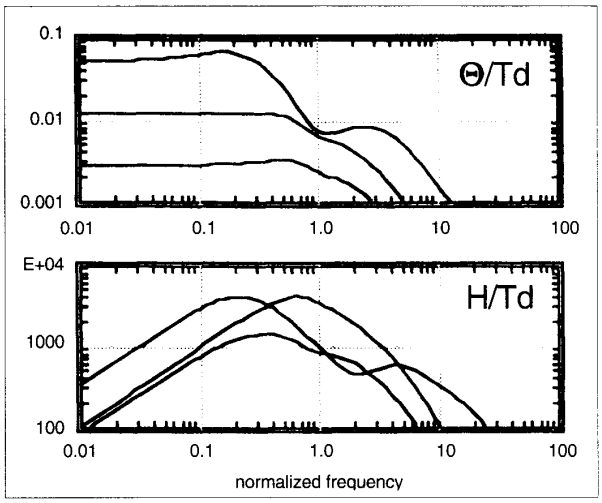

Fig. 6. Closed loop singular values, Design Trial 2.

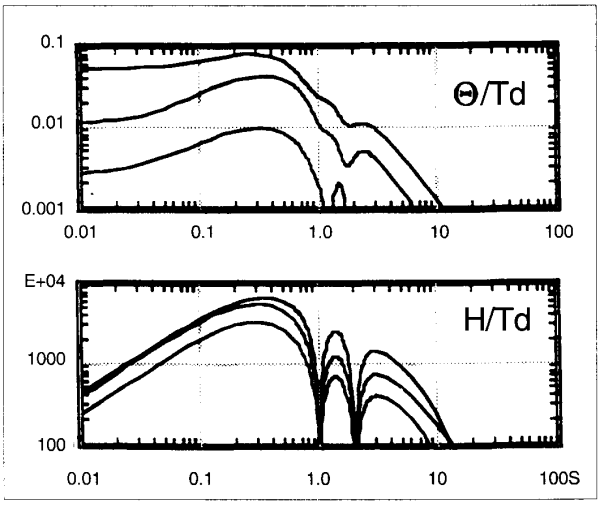

Fig. 8. Closed loop singular values, Design Trial 3.

penalty at other frequencies grows accordingly. Whether these additional disturbance rejection frequencies are actually needed depends upon predicted magnitudes of disturbance components for the final space station configuration. Since these predictions are still in flux, the current baseline control architecture is designed to remain flexible, making provisions for rejection frequencies up to several harmonics.

Simplified Controller Designs

While the H-infinity formalism provides an efficient way to conduct basic tradeoffs to generate preliminary station control laws, the H-infinity compensators themselves are quite complicated, requiring six measurements (nine when attitude rates are also used) to be cross-strapped to three control commands through a 30-state dynamic system (9 states originated from the rigid system dynamics, 15 from W_d weights in Trial 3, and 6 from W_a weights). Moreover, the functional dependencies of these compensators on the station's mass properties are difficult to trace, requiring nothing short of ground-based or on orbit Riccati iterations to update them as mass properties change.

In order to determine whether such ambitious implementations are indeed justified, a set of simpler alternate control laws have been designed and compared with the optimal compensators for performance and robustness properties. Results of these design efforts and comparisons are summarized below.

The simplified control laws are based on a common classical approach to spacecraft control design, namely the separation of tasks into a high-bandwidth inner loop for attitude control and another low-bandwidth outer loop generating attitude commands to achieve mission objectives (e.g., momentum management). This structure is illustrated in Fig. 9.

A key feature of this classical loop partition is that its individual elements reduce to very simple control design tasks. For example, the inner loop breaks into three separate control channels, comprised of SISO double integrator plants with principal moments of inertia (J_{xx}, J_{yy}, J_{zz}) as their major changing parameters. It follows that a standard PD control law, e.g.,

$$T_{cy} = J_{yy}\left[k_\theta(\theta_{cmd} - \theta) - k_\theta \frac{d\theta}{dt}\right] \tag{6}$$

suffices for each channel, provided that its bandwidth is high enough to overpower the low-frequency gravity gradient terms and gyroscopic interactions present in the full station dynamics. We find that 7 to 10 times orbit rate is a sufficient bandwidth. We also include roll-off filters in each channel to attenuate structural resonances. Note that the explicit appearance of moments of inertia in the PD control law makes it easy to schedule as a function of mass properties.

The outer loop momentum management also breaks into smaller subtasks. Specifically, basic linearized station dynamics show that pitch axis momentum is uncoupled from roll/yaw and obeys the following SISO transfer relations:

$$H_y = \frac{GG_y - J_{yy}s^2}{s} g(s)\, \theta_{cmd} \tag{7}$$

where $GG_y = 3\,\omega_0^2(J_{zz} - J_{xx}) > 0$ is the (destabilizing) pitch axis gravity gradient gain and g(s) is the transfer function of the closed inner loop from attitude command to attitude. Since $g(s) \approx 1$ at low frequencies, this equation shows that pitch axis momentum dynamics are dominated by a simple integrator with two zeros, one stable and one unstable, at frequencies near orbit rate. The non-minimum phase zero constrains outer loop bandwidth, and thus, it limits achievable momentum performance. This provides a classical explanation of why we were unable to make the station's momentum responses arbitrarily small.

Standard loop shaping methods lead to the following compensator for the plant in (7):

$$\theta_{cmd} = \frac{c_y}{GG_y}\frac{p}{(s+p)}\frac{(s+z)}{s} H_y \tag{8}$$

Here the term $(s + z)/s$ provides integral control with reset times determined by z, the term $p/(s + p)$ cancels the stable zero, and the gain level, c_y / GG_y, is set to achieve good crossover properties at a crossover frequency slightly below orbit rate. Note again that this compensator depends explicitly on the gravity gradient gain, making it easy to schedule as a function of changing mass properties.

Similar classical analyses have been performed for the station's coupled roll/yaw momentum components. With inner loops closed, these components obey the following transfer relation:

$$\begin{bmatrix} H_x \\ H_z \end{bmatrix} = \frac{J_{zz}}{s^2 + \omega_0^2}\begin{bmatrix} s(s^2 - 2\omega_0^2) & -\omega_0(s^2 + \omega_0^2) \\ \omega_0(s^2 + 4\omega_0^2) & s(s^2 + \omega_0^2) \end{bmatrix} g(s) \begin{bmatrix} \phi_{cmd} \\ \psi_{cmd} \end{bmatrix} \tag{9}$$

(For simplicity, we assume here that $J_{xx} \approx J_{zz}$ and $J_{yy} << J_{zz}$. These conditions are well satisfied in the assemble-complete configuration.) Equation (11) shows that roll/yaw momentum dynamics are dominated by a neutrally stable orbit rate oscillator, corresponding to the natural interchange of body-fixed roll and yaw momentum components as the station proceeds around its orbit. This oscillator can be stabilized by feeding back H_x to ϕ_{cmd}. The "plant" for this loop is the 11-element of the transfer matrix above, which provides the necessary rate signal but is bandwidth-constrained by a non-minimum phase zero slightly above orbit rate. (Again, we have a classical interpretation of momentum management limitations).

Because the 11-element has a zero at the origin, integral control for H_x cannot be obtained through the same feedback channel. However, we can cross-feed H_x through an integrator to ψ_{cmd} for the same effect. Similarly, we can cross-feed H_z to ϕ_{cmd} to achieve integral control of H_z. These considerations lead to the following simplified roll/yaw momentum controller:

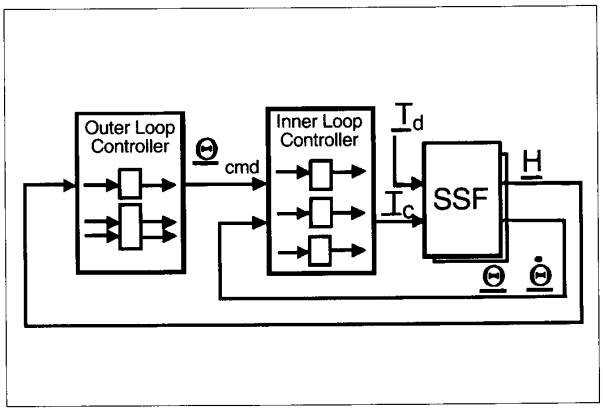

Fig. 9. Conventional inner/outer loop partition.

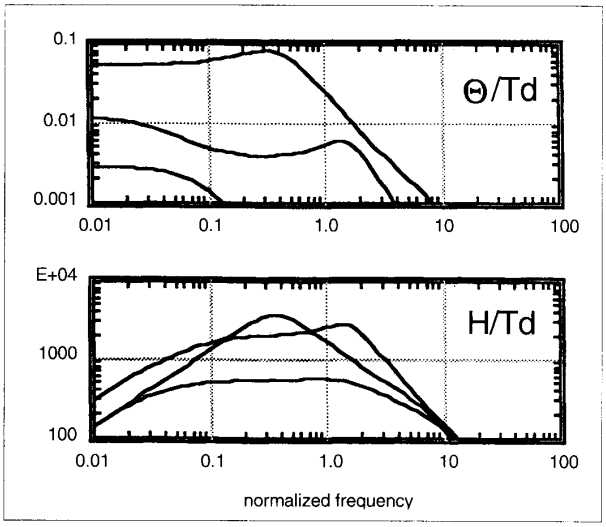

Fig. 10. Closed loop singular values for simplified controller (cy = −1, cx = −0.35, cxz = 0.02, czx = −0.04).

$$\begin{bmatrix}\phi_{cmd}\\ \psi_{cmd}\end{bmatrix} = \frac{1}{\omega_0 J_{zz}}\begin{bmatrix}\dfrac{c_x p}{s+p} & \dfrac{c_{xz}}{s}\\ \dfrac{c_{zx}}{s} & 0\end{bmatrix}\begin{bmatrix}H_x\\ H_z\end{bmatrix} \tag{10}$$

In this case, the $p/(s+p)$ term cancels the stable zero of the 11-element of the plant, constant c_y is selected for good crossover properties with crossover frequencies near orbit rate, and constant c_{xz} and c_{zx} are selected to produce reasonable integral control reset times (2-3 orbits). Again, the explicit dependence of this controller on J_{zz} makes it easy to schedule with changes in the station's mass properties.

The inner loop controllers from (6) together with the outer loop controllers from (8) and (10) produce the closed loop singular value frequency responses shown in Fig. 10. These responses should be compared with their H-infinity counterparts from Figure 6. Note that attitude and momentum responses are very similar for both designs. The simplified controller has slightly lower momentum peaks, purchased with somewhat larger attitudes. Evidently, near-optimal performance can be achieved by control structures which are significantly simpler than the optimal ones!

Simplified Disturbance Rejection Filters

While simplified controller designs for basic stabilization and DC disturbance rejection proved to be well suited to standard classical methods, the job of incorporating disturbance rejection capability at other discrete frequencies (as in Fig. 8) proved to be more difficult. The basic challenge is to create high outer loop gains at orbit rate and twice orbit rate, right in the vicinity of the non-minimum phase zeros of (7) and (9) Various *ad hoc* schemes for including resonances was attempted, with marginal success. Imitation proved to be the most successful alternative. We computed full H-infinity controllers for the outer loops, with weights chosen to produce disturbance rejection as in Design Trial 3. We then studied the resulting loop shapes, approximating their pole/zero patterns, and incorporating these in the simplified design.

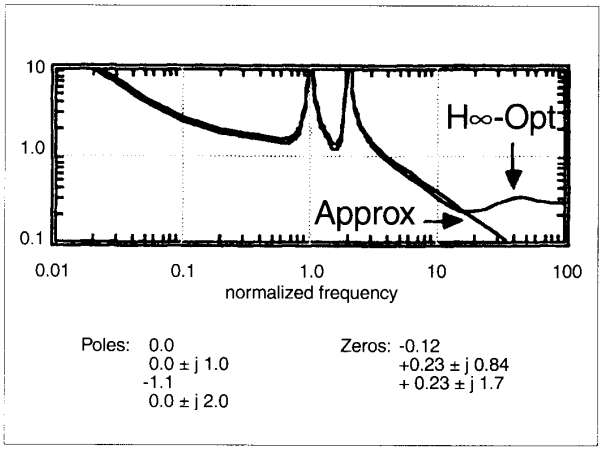

Fig. 11. Pitch axis outer loop control approximation.

An example of this approximation process is shown in Figs. 11-12. These figures apply to the pitch axis which experiences the largest disturbance torques (relative to inertia) and thus has the greatest need for disturbance rejection filters. Fig. 11 shows frequency responses of an H-infinity outer loop controller and of its pole-zero approximation. The figure also lists the poles and zeros. Note that the poles are resonant at orbit rate and twice orbit rate, as we would expect, but some of their associated zeros are non-minimum phase. Since examples where a controller must add additional non-minimum phaseness to an existing non-minimum phase plant are rare in classical design, it is easier to understand why our *ad hoc* methods failed to discover this alternative.

A comparison of the disturbance rejection properties of the full H-infinity outer loop and its simplified approximation is shown in Fig. 12. The comparison proves to be quite favorable.

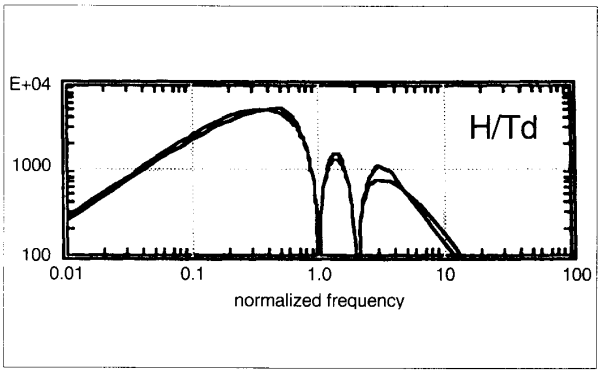

Fig. 12. Pitch axis outer loop control comparison.

Space Station Structured Singular Value Analysis

Structured singular value analysis is a technique for determining how large parameter variations can be before a linear control system becomes unstable. This section describes structured singular value (μ) analysis conducted to assess the robustness properties of the above control designs with respect to mass properties variations. References [3] and [6]-[8] are representative of earlier studies of the space station attitude/momentum dynamics that have analyzed these variations with μ

and other techniques. Since the moment of inertia variations are quite large, it is important to remove as much conservatism as possible by taking advantage of the known structure of the moment-of-inertia matrix.

We develop a perturbation structure which exactly represents the variations caused by a payload moving in a box shaped region. The perturbed system is put into the standard Δ, P, K format of μ-analysis described in [9]. The resulting Δ matrix has dimension 25×25. Given this perturbation structure, the structured singular values for the closed loop system are computed for each of the two control designs.

Moments of Inertia for the Composite Vehicle

The main body of the space station has mass m_1, moment-of-inertia J_1, and center of gravity $\underline{r}_{cg1}$. The payload has mass m_2, moment-of-inertia J_2, and center of gravity $\underline{r}_{cg2}$. Let

$$m = \frac{m_1 m_2}{m + m_2} \quad \text{and} \quad \begin{bmatrix} x \\ y \\ z \end{bmatrix} = \underline{r} = \underline{r}_{cg2} - \underline{r}_{cg1} \tag{11}$$

Define the "tilde" operator from 3-vectors to 3-by-3 skew-symmetric matrices as follows:

$$\tilde{\underline{r}} = \begin{bmatrix} 0 & -z & y \\ z & 0 & -x \\ -y & x & 0 \end{bmatrix} \tag{12}$$

Using this tilde operator, the change in moment of inertia J_{12} due to payload c.g. and vehicle c.g. being separated can be written in factored form:

$$J_{12} = -m\tilde{\underline{r}}^2 = m \begin{bmatrix} y^2+z^2 & -xy & -xz \\ -xy & x^2+z^2 & -yz \\ -xz & -yz & x^2+y^2 \end{bmatrix} \tag{13}$$

The combined moment of inertia of the system about the system cg is given by:

$$J = J_1 + J_2 + J_{12} \tag{14}$$

Mass Properties Variations and Perturbed System Dynamics

We will assume that J_1 and J_2 are both known, but that J_{12} can be anywhere in a range defined by the possible payload locations:

$$\underline{r} = \underline{r}_{ave} + \begin{bmatrix} \delta_x & 0 & 0 \\ 0 & \delta_y & 0 \\ 0 & 0 & \delta_z \end{bmatrix} \underline{r}_{diff} \qquad |\delta_i| <= 1 \quad i = x,y,z \tag{15}$$

The only dependence on J in the linearized dynamics comes from (5). Since $L(J)$ is linear in J:

$$L(J) = L(J_1 + J_2) + L(J_{12}) \tag{16}$$

so the linearized dynamics can be written as

$$(J_1 + J_2 + J_{12})\,\ddot{\underline{\theta}} = \left(L(J_1 + J_2) + L(J_{12})\right) \begin{bmatrix} \omega_0 \dot{\underline{\theta}} \\ \omega_0^2 \underline{\theta} \end{bmatrix} - \underline{T} \tag{17}$$

Putting the MOI and Torque Matrices into Linear Fractional Form

Linear fractional transformations (LFTs) are rational functions whose numerator and denominator are both linear (possibly matrix) functions. Their use in describing uncertainties in linear systems is described in [10].

J_{12} has only three independent parameters, (x, y, and z), so we must write J_{12} and $L(J_{12})$ as linear fractional transformations with respect to them. The first step is to write J_{12} and $L(J_{12})$ as explicit functions of (x,y,z). Equation (13) already gives J_{12} as an explicit quadratic function of (x,y,z). Reference [11] shows how to write L (J_{12}) as an explicit quadratic function of x,y,z.

Polynomial (or even rational) matrix functions in several variables can be put directly into the linear fractional format, however the dimension of the required uncertainty matrix can be very large. A preliminary description of these techniques is given in [12]. The direct representation of an $n \times m$ matrix which is quadratic in k independent δs requires an uncertainty matrix with $(n+m)*k$ δs on the diagonal. In our case, there are 3 independent δs, so the direct implementation of $L(J_{12})$ as an LFT requires 27 δs. References [11] and [13] contain detailed derivations of this perturbation structure. In addition, it takes 18 δs to represent J (or J^{-1}) as an LFT. The total number of δs required is 45.

In order to reduce the dimension of the uncertainty matrix, it is sometimes useful to first factor the matrix polynomials. Polynomial functions in several variables cannot always be factored into linear terms, however in our case this is possible. Once the factors are found, they can be represented with a minimal number of δs using the singular value decomposition as described in [14]-[15].

Factoring the MOI and Torque Matrices

J_{12} is already in factored form (see (13)). The 3×6 matrix $L(J_{12})$ can also be factored into left and right factors each of which is linear in x, y, and z:

$$L(J_{12}) = m\tilde{\underline{r}} \begin{bmatrix} 2y & 0 & 0 & 0 & -3z & -y \\ 0 & 2y & 0 & 4z & 0 & -x \\ 0 & 0 & 2y & 4y & -3x & 0 \end{bmatrix} \tag{18}$$

The factors are not unique, as noted in [13]. The physical interpretation of the factorization is that the torques produced on the system by the extended payload can be expressed as $\underline{r} \times \underline{\text{force}}$ where the force is a

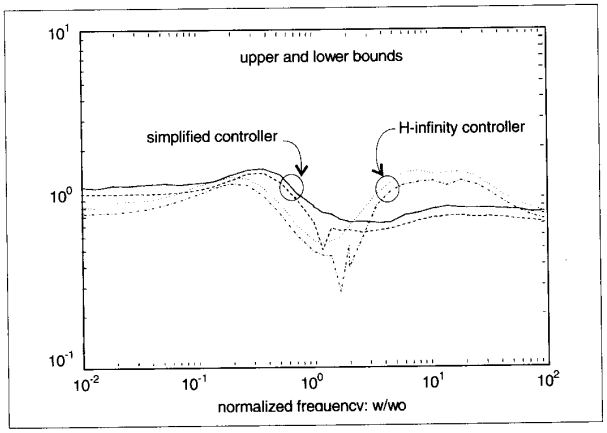

Fig. 13. Mu plots.

linear function of $\underline{r}$. The nonuniqueness of the factorization is due to the fact that an arbitrary additional force in the direction of $\underline{r}$ can be added without affecting the torque cross product.

The factors can be put into linear fractional form of minimal order using the techniques described in [14]-[15].

Adding, subtracting, multiplying, and inverting LFTs results in another LFT (using the standard formulas for adding, subtracting, multiplying, and inverting system matrices). The matrix $J^{-1}L(J)$ can be obtained by adding, subtracting, multiplying, and inverting the LFTs for its linear factors. Therefore $J^{-1}L(J)$ can be obtained as an LFT with respect to $(\delta_x, \delta_y, \delta_z)$.

This factorization approach requires 13 δs for $L(J)$ and 12 δs for J^{-1}, giving a total of 25 δs. This compares well with the direct implementation of the unfactored $L(J)$ and J^{-1} which required a total of 45 δs.

Numerical Computations

It is difficult to calculate μ exactly; however, there are numerical algorithms for computing upper and lower bounds. The lower bound for complex μ was computed using the Power Method described in [17]. The upper bound was computed using the Osborne Method modified to allow repeated scalar blocks, as described in [18].

Using the factored perturbation structure, we computed the structured singular values of the closed loop systems obtained using the controllers described in earlier sections. A payload mass was allowed to be anywhere in the range given by:

$$\underline{r}_{\text{ave}} = \begin{bmatrix} 0.072 \\ 0 \\ 0 \end{bmatrix} \sqrt{J_z/m} \qquad \underline{r}_{\text{diff}} = \begin{bmatrix} 0.072 \\ 0.288 \\ 0.144 \end{bmatrix} \sqrt{J_z/m} \tag{19}$$

Fig. 13 shows that the controller designed using H-infinity and the simplified controller have essentially the same robustness properties. The upper and lower bounds for complex μ were computed using μ-Tools [16]. Since $\mu \approx 1.4$, the system is robustly stable for all payload positions that are 1/1.4 as large as those given in (19). Complex μ is conservative since it assumes complex perturbations are possible, while the moment of inertia perturbations are clearly real. To see how this conservatism affected our results, we also computed upper and lower bounds for real perturbations using a branch and bound algorithm given in [19]. For the simplified controller, the branch and bound algorithm showed that the system was stable for perturbation 0.5 times as large as those given in (19), and the system was unstable for perturbations 0.75 times as large as those in (19). Sharper ranges can be obtained with more computing time, but are not available yet.

Further Work

The H-infinity controller and the simplified controller have very similar performance and robustness properties. We are currently applying these controllers to the various build sequences and flight orientations of the space station. We are also applying complex and real parameter variation algorithms to the robust performance problem.

Acknowledgement

The authors would like to thank Blaise Morton, Neal Flanagan, David Chang, and Jim Mullins for their help on this project.

References

[1] S. R. Vadali and H.-S. Oh, "Space station attitude control and momentum management: A nonlinear look," *J. Guidance, Control, Dynam.*, May-June 1992.

[2] J. Yeichner, J. Lee, and D. Barrows, "Overview of space station attitude control system with active momentum management," presented at 11th Annual AAS Guidance and Control Conf., 1988.

[3] B. Wie, K. W. Byun, W. Warren, D. Geller, D. Long, and J. Sunkel, "New approach to attitude/momentum control of the space station," *J. Guidance, Control, Dynam.*, vol. 12, no. 5, pp. 714–722, 1989.

[4] J. Doyle, K. Glover, P. Khargonekar, and B. Francis, "State-space solutions to standard H_2 and H-infinity control problems," *IEEE Trans. Auto. Control*, vol. AC-34, no. 8, 1988.

[5] J. Harduvel, "Continuous momentum management of earth-oriented spacecraft," presented at AIAA Guidance Navigation and Control Conf., Portland, OR, Aug. 20–22, 1990.

[6] K. W. Byun, B. Wie, D. Geller, and J. Sunkel, "Robust H-infinity control design for the space station with structured parameter uncertainty," presented at AIAA Guidance Navigation and Control Conf., Portland, OR, Aug. 20–22, 1990.

[7] G. Balas, A. Packard, and J. Harduvel, "Applications of mu-synthesis techniques to momentum management and attitude control of the space station," presented at AIAA Guidance, Navigation and Control Conf., Jan. 1991.

[8] I. Rhee and J. Speyer, "A game theoretic controller for a linear time-invariant system with parameter uncertainty and its application to the space station," presented at AIAA Guidance Navigation and Control Conf., Portland, OR, Aug. 20–22, 1990.

[9] G. Stein and J. Doyle, "Beyond singular values and loop shapes," *J. Guidance*, vol. 14, no. 1, Jan.-Feb. 1991.

[10] J. Doyle, A. Packard, and K. Zhou, "Review of LFT's, LMI's and mu," in *Proc. IEEE Conf. Decision and Control*, Brighton, England, 1991.

[11] M. Elgersma, G. Stein, M. Jackson, and J. Yeichner, "Robust controllers for space station momentum management," in *Proc. IEEE Conf. Decision and Control*, Brighton, England, 1991.

[12] K. Zhou and J. Doyle, "Notes on MIMO control theory," 1990, unpublished.

[13] J. Doyle, B. Morton, and M. Elgersma, "New methods in robust control," Final Tech. Rep., AFOSR Contract F49620-88C-0077, Oct. 1991.

[14] B. Morton, "New applications of μ to real parameter variation problems," in *Proc. IEEE Conf. Decision and Control*, 1985.

[15] K. W. Byun, B. Wie, and J. Sunkel, "Robust control synthesis for uncertain dynamical systems," *J. Guidance, Control, Dynam.*, submitted for publication.

[16] G. Balas, J. Doyle, K. Glover, A. Packard, and R. Smith, "mu-tools: The mu-analysis and synthesis toolbox," MUSYN Inc. and The Mathworks, Apr. 1991.

[17] A. Packard and J. Doyle, "Structured singular value with repeated scalar blocks," in *Proc. Amer. Control Conf.*, Atlanta, GA, 1988, pp. 1213-1218.

[18] A. Packard, M. Fan, and J. Doyle, "A power method for the structured singular value," in *Proc. IEEE Conf. Decision and Control*, Austin, TX, Dec. 1988, pp. 2132-2137.

[19] V. Balakrishnan, S. Boyd, and S. Balemi, "Branch and bound algorithm for computing the minimum stability degree of parameter-dependent linear systems," *Int. J. Robust Nonlinear Control*, submitted for publication.

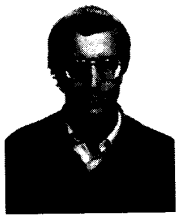

Michael R. Elgersma received the B.E.E. and M.S.E.E. degrees in electrical engineering and the Ph.D. degree in control science and dynamical systems from the University of Minnesota, Minneapolis, MN, in 1981, 1986, and 1988, respectively. From 1979 through 1981, he was with Honeywell Military Avionics Division, and since 1981 he has been with Honeywell Systems and Research Center, both in Minneapolis, MN. His current research areas include real parameter variations, nonlinear control, and multibody dynamics.

Gunter Stein received the B.S.E.E. degree from GMI, Flint, MI, and the M.S.E.E. and Ph.D. degrees from Purdue University, West Lafayette, IN, in 1966 and 1969 respectively. Since 1969, he has been with Honeywell Systems and Research Center, Minneapolis, MN, where he currently holds the position of Chief Scientist. He is also Adjunct Professor in Electrical Engineering and Computer Science at the Massachusetts Institute of Technology, Cambridge. He is a fellow of the IEEE.

Michael R. Jackson received the B.S. degree in 1987 and the M.S. degree in 1989, both in aerospace engineering, from the University of Minnesota Institute of Technology. Since 1987, he has been with Honeywell Systems and Research Center, Minneapolis, Minnesota. His current research areas include embedded software architectures for reliable GN&C systems, and Space Station Freedom attitude control. Previously, he was working on guidance methods for the National Aerospace Plane (NASP).

John Yeichner received the B.E.E. and M.S. degrees in engineering from The Ohio State University in 1966 and 1969, respectively. He is a Senior Project Staff Engineer at Honeywell's Space and Strategic Systems Operation in Clearwater, Florida. He is currently responsible for leading the design and development of the CMG/Momentum Management Attitude Control System (ACS) for NASA's Space Station Freedom. He was also involved in the design of the Flight Control System for NASA's Space Shuttle. While employed by the Bendix Corporation, he was involved in the design of the CMG Attitude Control System for NASA's first space station, SKYLAB.

Out of Control

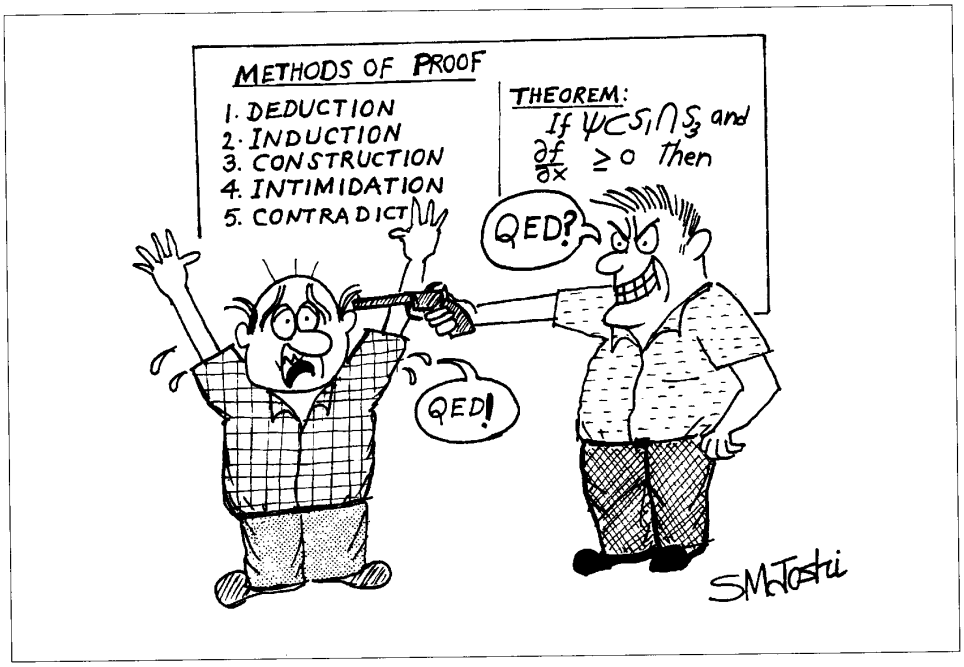

Professor Kudthroat proves a theorem by the fourth method.